HHS Public Access

Author manuscript

Cell Rep. Author manuscript; available in PMC 2021 April 02.

Published in final edited form as:

Cell Rep. 2019 July 23; 28(4): 923–937.e3. doi:10.1016/j.celrep.2019.06.069.

Constitutive Activation of the B Cell Receptor Underlies Dysfunctional Signaling in Chronic Lymphocytic Leukemia

Carly G.K. Ziegler[1,2,7,*], **Joel Kim**[1,2], **Kelly Piersanti**[2,4], **Alon Oyler-Yaniv**[1,6], **Kimon V. Argyropoulos**[2,3], **Marcel R.M. van den Brink**[2,3], **M. Lia Palomba**[2,4], **Nihal Altan-Bonnet**[5], **Grégoire Altan-Bonnet**[1,2,8,9,*]

[1]ImmunoDynamics Group, Programs in Computational Biology and Immunology, Memorial Sloan Kettering Cancer Center, New York, NY 10065, USA

[2]Center for Cancer Systems Biology, Memorial Sloan Kettering Cancer Center, New York, NY 10065, USA

[3]Department of Medicine and Immunology Program, Memorial Sloan Kettering Cancer Center, New York, NY 10065, USA

[4]Lymphoma Service, Department of Medicine, Memorial Sloan Kettering Cancer Center, New York, NY 10065, USA

[5]National Heart, Lung, and Blood Institute, NIH, Bethesda, MD 20892, USA

[6]Physics Department, Ben Gurion University, Beer-Sheva, Israel

[7]Present address: Harvard-MIT Division of Health Sciences and Technology, Harvard Medical School, Boston, MA 02139, USA

[8]Present address: ImmunoDynamics Group, Center for Cancer Research, National Cancer Institute, Bethesda, MD 20892, USA

[9]Lead Contact

SUMMARY

In cancer biology, the functional interpretation of genomic alterations is critical to achieve the promise of genomic profiling in the clinic. For chronic lymphocytic leukemia (CLL), a heterogeneous disease of B-lymphocytes maturing under constitutive B cell receptor (BCR)

*Correspondence: carly_ziegler@hms.harvard.edu (C.G.K.Z.), gregoire.altan-bonnet@nih.gov (G.A.-B.).

AUTHOR CONTRIBUTIONS

C.G.K.Z. and G.A.-B. conceived and designed the experiments; C.G.K.Z., J.K., and G.A.-B. performed the experiments; C.G.K.Z. and G.A.-B. developed the computational model; C.G.K.Z., J.K., A.O.-Y., M.L.P., N.A.-B., and G.A.-B. analyzed the data: K.V.A. and M.R.M.v.d.B. contributed reagents and materials; and C.G.K.Z., N.A.-B., and G.A.-B. wrote the paper.

DECLARATION OF INTERESTS

M.R.M.v.d.B. has received research support from Seres Therapeutics; has consulted for, received honoraria from, or participated in advisory boards for Seres Therapeutics, Flagship Ventures, Novartis, Evelo, Jazz Pharmaceuticals, Therakos, Amgen, Merck, Acute Leukemia Forum (ALF), Magenta, and DKMS Medical Council (board only); and has intellectual property (IP) licensing with Seres Therapeutics and Juno Therapeutics. M.L.P. has consulted for Merck and Pharmacyclics. The other authors declare no competing interests.

SUPPLEMENTAL INFORMATION

Supplemental Information can be found online at https://doi.org/10.1016/j.celrep.2019.06.069.

stimulation, the functional role of diverse clonal mutations remains largely unknown. Here, we demonstrate that alterations in BCR signaling dynamics underlie the progression of B cells toward malignancy. We reveal emergent dynamic features—bimodality, hypersensitivity, and hysteresis—in the BCR signaling pathway of primary CLL B cells. These signaling abnormalities in CLL quantitatively derive from BCR clustering and constitutive signaling with positive feedback reinforcement, as demonstrated through single-cell analysis of phospho-responses, computational modeling, and super-resolution imaging. Such dysregulated signaling segregates CLL patients by disease severity and clinical presentation. These findings provide a quantitative framework and methodology to assess complex and heterogeneous leukemia pathology and to inform therapeutic strategies in parallel with genomic profiling.

Graphical Abstract

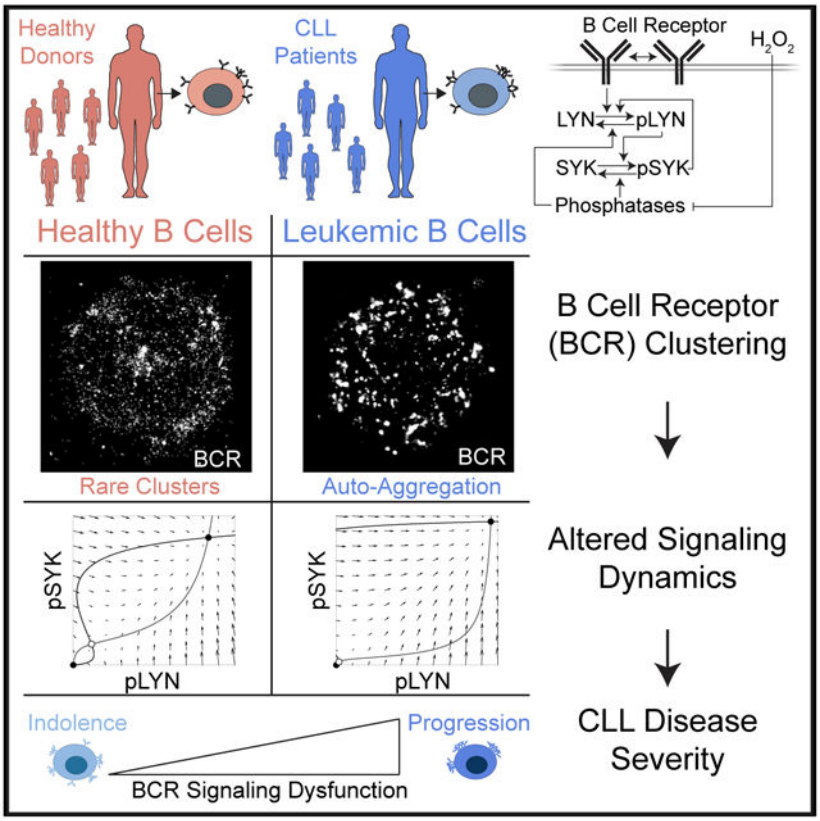

In Brief

Using phospho-flow cytometry and computational modeling, Ziegler et al. find that B cell receptor clustering and positive feedback through SYK and LYN drive signaling hypersensitivity, bistability, and hysteresis in chronic lymphocytic leukemic B cells. Super-resolution microscopy confirms membrane auto-aggregation in leukemic B cells, and variability in signaling dysfunction predicts disease severity.

INTRODUCTION

B cell survival, proliferation, and response to antigen relies on robust and tightly regulated activation of the B cell receptor (BCR) signaling pathway, initiated by engagement and multimerization of the BCR within a signaling complex. Recent studies have demonstrated that in chronic lymphocytic leukemia (CLL), a B cell neoplasm, the BCRs from malignant cells have the capacity to activate the BCR-proximal signaling pathway in a cell-autonomous manner (Binder et al., 2013; Dühren-von Minden et al., 2012). The emerging paradigm states that CLL B cells possess a cell-intrinsic capacity for auto-activation, and this alteration underlies oncogenic transformation and progression. Accordingly, studies of gene expression and signal transduction have consistently supported an “activated” phenotype among CLL B cells and suggested a link between cellular activation and disease progression. Functional snapshots of the CLL B cell phenotype suggest that CLL is a disease of skewed cellular physiology, in which cells become aberrantly “stuck” in a hyperactive state, akin to the signaling phenotypes of antigen-experienced B cells (Damle et al., 2002; Klein et al., 2001; Minici et al., 2017). However, sequencing of CLL B cells has failed to identify universally shared, signaling-relevant mutations in their BCR (Agathangelidis et al., 2012; Hoogeboom et al., 2013) or genetic alterations among signaling components downstream of BCR (Landau et al., 2013; Nadeu et al., 2016). Hence, we hypothesized that a common disease etiology may exist as subtle and varied genomic alterations in the BCR, which may shift the dynamics of BCR signaling and underlie the altered physiology of CLL B cells in their malignant states.

Constitutive clustering of the BCR has been observed in an activated B cell-like subtype of diffuse large B cell lymphoma (Davis et al., 2010) and CLL (Gomes de Castro et al., 2019). Similar clustering upon antigen engagement in normal B cells (Harwood and Batista, 2010; Ketchum et al., 2014; Lee et al., 2017) drives the assembly of a signalosome, with the phosphorylation of BCR-associated chains and the accretion and phosphorylation of kinases such as spleen tyrosine kinase (SYK), phospholipase-Cγ2 (PLCγ2), Bruton’s tyrosine kinase (BTK), and adaptor molecules such as B cell linker (BLNK). In this context, multivalent soluble antigens are far more potent in eliciting B cell signaling compared to monovalent antigens (Harwood and Batista, 2010); cytoskeletal depolymerization fluidifies the membrane, renders the BCR more mobile, and drives activation (Ketchum et al., 2014), such that any clustering of surface BCRs can trigger a phosphorylation cascade. Alternatively, Reth and coworkers have proposed a model whereby oligomerization of the BCR occurs even in resting B cells and is critical to regulate signaling responses by auto-inhibition (Yang and Reth, 2010a, 2010b). Overall, we conjecture that cell-autonomous BCR signaling in CLL lymphoma may relate to biophysical alterations in the BCR on the cell membrane, affecting dynamic behavior of the BCR-associated signalosome.

Single-cell proteomics has emerged in tandem with advanced genomic methods, with great promise to characterize the signaling responses and physiology of clinical samples (Irish et al., 2004). To provide functional context to observed genomic lesions in any cancer specimen, methods must be developed to integrate measurements of the signaling and differentiation status of biological and clinical samples at the single-cell level. Achieving such single-cell resolution in the study of biological systems has long been recognized as an

important step toward a quantitative understanding of biological responses, in particular when dissecting the phenotypic variability of cells within isogenic populations and identifying the most central mechanisms and factors in biological regulation (Cotari et al., 2013b; Feinerman et al., 2008; Krishnaswamy et al., 2014).

Developmental biologists have already leveraged quantitative modeling at single-cell resolution in the study of emergent properties of biological systems. For example, the observation and manipulation of *Xenopus* oocytes at the single-cell level led to the discovery of the dynamics and mechanisms controlling the all-or-none commitment of individual eggs to enter mitosis (Ferrell and Machleder, 1998). Similar observations of bimodality in biological responses were reproduced for cells undergoing apoptosis (Spencer et al., 2009) or for lymphocytes responding to antigens (Altan-Bonnet and Germain, 2005; Das et al., 2009). Exquisite control of threshold-based, switch-like behavior is ubiquitous across biological systems, yet such observations are challenging to dissect at the molecular level and hard to interpret in their ability to generate functional cell-to-cell heterogeneity (Feinerman et al., 2008; Vogel et al., 2016). In CLL, prior efforts have succeeded in using statistical methods to understand cellular heterogeneity by classifying clinical samples according to genomic or proteomic data (Damle et al., 1999; Döhner et al., 2000). However, full elucidation of the mechanistic molecular changes that drive clinical variability must use a “bottom-up” approach, relying on the precise characterization of protein-protein molecular events, biochemical models that reduce the complexity of signaling networks, and integration of high-dimensional data obtained from flow cytometry and other methods into a reductionist representation (Gunawardena, 2014; Machta et al., 2013).

In this study, we apply quantitative single-cell analysis to experimentally interrogate and theoretically model signal transduction in primary B cells from CLL patients and healthy donors. We observe that B cells respond in an all-or-none manner to phosphatase inhibition; we attribute this emergent behavior to SYK-kinase-dependent positive feedback, based on theoretical modeling of signaling responses in single cells and validated using small molecule inhibitors. Moreover, we demonstrate that unique B cells respond to phosphatase inhibition with hysteresis—they exhibit “memory” of prior signaling activation. As a cohort, primary tumor cells from CLL patients display robust enhancement in their response to stimuli: lower thresholds to all-or-none activation and more pronounced hysteresis, often with stable stimulus-independent activation. We introduce a mathematical model of signaling dynamics that analyzes mechanisms to generate signaling diversity through the alteration of biological entities (e.g., BCR clustering) and/or variable biochemical parameters (e.g., protein abundance and noise). We directly test these theoretical insights on a cohort of patient-derived tumor samples. As predicted by model simulations, varying degrees of constitutive signaling explain the diversity in cellular activation phenotypes from different patients with CLL. We validate this observation using biophysical and signaling assays and direct quantification of BCR constitutive multimerization using super-resolution microscopy. Finally, BCR multimerization and signaling dysfunction strongly predict clinical severity in CLL and other B cell leukemias. Hence, by unifying single-cell phosphoproteomic studies with mathematical modeling, we uncover a dysfunctional cellular behavior that underlies disease severity in primary B cell neoplasia.

RESULTS

Single-Cell Analysis of B Cells upon Phosphatase Inhibition Reveals Bimodality and Hysteresis of Kinase Activation

We developed an *ex vivo* assay to probe the signaling capacities of primary B cells collected from CLL patients and healthy donors (see Table S1 for donor characteristics). We exposed peripheral blood mononuclear cells (PBMCs) to different concentrations of hydrogen peroxide (H_2O_2), an oxidizing agent that universally inhibits phosphatases in living cells (Khalil et al., 2012), for varying durations. We analyzed the BCR-proximal signaling response by quantifying the amount of phosphorylated LYN, SYK, and PLCγ2 kinases with single-cell resolution using flow cytometry (Figures 1A, 1B, S1A, and S1B) (Feinerman et al., 2008; Irish et al., 2004). Canonically, LYN kinase is responsible for mediating initial phosphorylation of the conserved tyrosine residues on immunoglobulin α/β (Igα/β) cytoplasmic domains, providing docking sites for other associated kinases such as FYN, CSK, and SYK. SYK engages with phosphorylated tyrosines via tandem SH2 domains and mediates additional phosphorylation events, leading to the assembly of a membrane-proximal signalosome with diverse downstream outcomes of activation, including phosphatidylinositol 3-kinase (PI3K) activation, BTK recruitment and phosphorylation, and PLCγ2 phosphorylation. We observed that the response of primary B cells to stimulation (from both CLL patients and healthy donors) is strictly bimodal. For increasing concentrations of H_2O_2, the fraction of activated B cells increases, but the mode of the distribution of phosphorylated kinases (LYN, SYK, PLCγ2) remains unchanged (i.e., the quantity of phosphorylated kinase per cell is the same in all activated cells). This is in striking contrast to the graded and analog pLCK response within T cells from the same PBMC pool (Figures 1B and S1B). To fully characterize the kinetics and dynamics of B cell stimulation, we assessed the degree of responsiveness of B cells to increasing concentrations of phosphatase-inhibiting H_2O_2 by measuring EC_{50}^{up} as the concentration of H_2O_2 that yielded 50% of the maximal fraction of SYK-phosphorylated B cells (Figures 1C, left panel, and 1E). CLL B cells are more sensitive to phosphatase inhibition ($EC_{50}^{up} = 4.4 \pm 0.9mM$), compared to B cells from healthy donors ($EC_{50}^{up} = 19 \pm 0.5mM$). Similar results were also obtained using sodium pervanadate, an alternate pan-phosphatase inhibitor (Figure S1C).

The kinetics of activation from rest and the threshold for stimulation only represent a subset of the dynamic properties of any signaling network. To further characterize this system, we next assessed the "relaxation" kinetics from full activation. We set healthy PBMCs into a highly activated state by exposing them to 30 mM H_2O_2 for 4 min, washing with complete RPMI, and exposing these pre-activated cells to lower concentrations of H_2O_2 to establish new steady states over 30 min (Figure 1C, right panel). As before, dephosphorylation of kinases by titrated reactivation of phosphatases proceeded in a digital fashion, with switch-like toggling of the whole-cell activation phenotype (Figure 1D). Among B cells from healthy donors, we found $EC_{50}^{down} = 3.6 \pm 0.5mM$ compared to $EC_{50}^{up} = 19 \pm 0.5mM$. This gap in the response of cells to increasing and decreasing doses of H_2O_2 is called hysteresis (Das et al., 2009; Mukherjee et al., 2013). This dynamic property is the hallmark of a system

whose state of activation is dependent on its perturbation history. Hysteresis is therefore an important factor in determining the contextual behavior for the signaling and cellular network of lymphocytes *in vivo*. A system whose intrinsic activation structure is highly sensitive to prior stimuli exhibits a memory of recent cellular context, making it inherently tunable by cell-specific microenvironmental stimuli (Das et al., 2009).

We found that B cells from CLL donors also display hysteresis in their phosphorylation of BCR signaling components (Figures 1C and 1D). An assessment of a cohort of CLL patients found that tumor clones responded to decreasing doses of H_2O_2 ("relaxation" from activation) with a substantially lower EC_{50}^{down} compared to healthy B cells. In a majority of CLL samples, a large fraction of the neoplastic cells remained activated 30 min after the complete washout of H_2O_2 (Figures 1D, right panel, S1D, and S1E). To quantify hysteresis in CLL B cells, we defined $\%\ pSYK^{+}_{hysteresis}$ as the percentage of B cells that remain SYK phosphorylated 30 min after phosphatase reactivation. We found that $\%\ pSYK^{+}_{hysteresis}$ is practically null for B cells from healthy donors ($\%\ pSYK^{+}_{hysteresis} = 6.5 \pm 0.74$), while it is large and variable for CLL B cells ($\%\ pSYK^{+}_{hysteresis} = 75.2 \pm 4.11$) (Figure 1F). Crucially, we found that stimulus-free activation in CLL B cells is independent of the magnitude of H_2O_2 applied (Figures S1E and S1F).

By assaying CLL B cell signaling with single-cell resolution, we established that the magnitude of phosphatase inhibition determines the fraction of cells that pass the threshold for activation, and highly activated cells remain phosphorylated independent of reactivated membrane-proximal phosphatases. We observe that CLL B cells and healthy B cells differ in hypersensitivity (responsiveness of kinase phosphorylation from rest) and hysteresis (stimulus-free activation) in the phosphorylation patterns of the BCR signaling pathway upon phosphatase inhibition. Moreover, these quantitative readouts, as summarized in Figures 1E and 1F, uncover and describe substantial variability between CLL patients.

Small Molecule Inhibitors Identify SYK as Responsible for Enforcing Positive Feedback in BCR Signaling

Bistability and hysteresis in the response of cells to normal biological stimuli are the hallmarks of positive feedback regulation (Das et al., 2009). We used small molecule inhibitors against the BCR-associated tyrosine kinases LYN and SYK to confirm the existence of and rigorously characterize a potential molecular mechanism for positive feedback in the BCR signaling pathway. Pretreating cells with either a Src-family kinase (SFK) inhibitor (PP2), which targets LYN, or a SYK inhibitor (R406) before stimulating cells by phosphatase inhibition (H_2O_2 exposure) decreased both the frequency of cells responding to phosphatase inhibition and the per-cell abundance of pLYN, pSYK, and pPLCγ2 (Figures 2A, 2B, and S2A-S2C). This demonstrates that B cells depend on active SYK and LYN kinase for downstream phosphorylation and cellular activation when perturbed from a resting state. Next, we treated B cells with tyrosine kinase inhibitors after activation by H_2O_2 exposure, which we previously observed induces hysteresis in this signaling network. We found that SFK activity was not required to maintain CLL B cells in their activated state, while SYK kinase activity was critical to sustain the phosphorylation of

LYN, SYK, and PLCγ2 in CLL B cells (Figures 2C and S2C). These data suggest that SYK acts as robust positive feedback onto the BCR-associated tyrosine kinases LYN and SYK (Kläsener et al., 2014). Furthermore, these data support our hypothesis that SYK-mediated feedback accounts for the digital mode of activation in the BCR pathway, the partial hysteresis as measured by EC_{50}^{down} in healthy donors, and the maintenance of CLL B cells in an active state, even after stimulus removal ($\% pSYK^{+}_{hysteresis} \gg 0$).

A Computational Model of Early Events in BCR Signaling Explains How Variability in Constitutive BCR Activation Generates Heterogeneity in B Cell Signaling

We developed a computational model of the proximal signaling events to deconvolve the modulation of phosphorylation by constitutive signaling and phosphatase inhibition (Figure 3A). Our computational model was built on previous modeling efforts in B cell signaling (Das et al., 2009; Mukherjee et al., 2013) and focused on the specific dynamics of LYN and SYK phosphorylation upon phosphatase inhibition by H_2O_2 treatment. Our computational goals were as follows:

1. To account for the bimodal distribution of pLYN and pSYK upon exposure to H_2O_2
2. To account for hysteresis in LYN and SYK phosphorylation upon the addition and removal of H_2O_2
3. To account for the cell-to-cell variability in phosphorylation patterns
4. To account for the donor-to-donor and disease-to-healthy variability in B cell responsiveness and hysteresis

Using a modified single-cell phosphorylation assay, we observed that the variability in EC_{50}^{up} between CLL and healthy B cells was eliminated when tonic signaling through the BCR was maximized via the complete saturation of surface Ig with bivalent anti-human IgM $F(ab')_2$ (Figure S3A). Therefore, we hypothesized that we could model the signaling networks and kinetic parameters downstream of the BCR as functionally identical. Additionally, this suggested that by altering the level of constitutive signaling (based on differential BCR clustering), we could eliminate the signaling differences between CLL B cells and B cells from healthy donors. Altered constitutive BCR signaling would, in theory, enable differential responsiveness to phosphatase (PTPx) inhibition. We also implemented the signaling feedback uncovered in Figure 2, which supports pSYK driving further LYN and SYK phosphorylation, to account for the bimodality and hysteresis in pLYN and pSYK.

We modeled the effective concentration of active phosphatase $[PTPx]_{active}$ within an individual cell as titrated down upon the addition of H_2O_2:

$$[PTPx]_{active} = \frac{1}{1 + \frac{k_{oxidize}}{k_{reduce}} \cdot [H_2O_2]} \cdot [PTPx]_{total}.$$

We calibrated the scaling between intracellular concentrations of H_2O_2 and varied extracellular concentrations (data not shown). Oxidation and reduction parameters were measured directly within our experiments using a cell-permeable fluorogenic dye, dichlorofluorescin diacetate (DCFDA), which detects hydroxyl, peroxyl, and other reactive oxygen species within primary B cells (Table 1; Figure S1D).

Oxidation of active phosphatases reduces the dephosphorylation rates for pLYN and pSYK and allows further LYN and SYK phosphorylation. To parameterize these dynamic equations, we built upon previous modeling studies (Mukherjee et al., 2013) and ad hoc measurements on our primary samples (Table 1). Our model represents the phosphorylation and dephosphorylation reactions for pLYN and pSYK:

$$\begin{cases} \frac{d[pLyn]}{dt} = -R^{pLyn}_{dephosphorylation} \\ \qquad\qquad +R^{pLyn}_{phosphorylation}(pSyk \rightarrow pLyn) \\ \qquad\qquad +R^{constitutive}_{phosphorylation}(BCR^* \rightarrow pLyn) \\ \frac{d[pSyk]}{dt} = -R^{pSyk}_{dephosphorylation} \\ \qquad\qquad +R^{pSyk}_{phosphorylation}(pLyn \rightarrow pSyk) \\ \qquad\qquad +R^{pSyk}_{phosphorylation}(pSyk \rightarrow pSyk) \end{cases}$$

$$\Rightarrow$$

$$\begin{cases} \frac{d[pLyn]}{dt} = -k^P_{cat}\frac{[pLyn]}{K^p_m + [pLyn]}[PTPx]_{active} + ([Lyn]_{total} - [pLyn]) \times \left(\frac{k^{pLyn}_{cat}}{K^{BCR-Lyn}_m} \cdot BCR^* + \frac{k^{pSyk}_{cat}}{K^{pSyk-Lyn}_m} \cdot \frac{k^{pSyk-BCR}_{on}}{k^{pSyk-BCR}_{off}} \cdot [pSyk] \cdot BCR^* \right) \\ \frac{d[pSyk]}{dt} = -k^P_{cat}\frac{[pSyk]}{K^p_m + [pSyk]}[PTPx]_{active} + ([Syk]_{total} - [pSyk]) \times \left(\frac{k^{pLyn}_{cat}}{K^{pLyn-Syk}_m} \cdot \frac{k^{pLyn-BCR}_{on}}{k^{pLyn-BCR}_{off}} \cdot [pLyn] \cdot BCR^* + \frac{k^{pSyk}_{cat}}{K^{pSyk-Syk}_m} \cdot \frac{k^{pSyk-BCR}_{on}}{k^{pSyk-BCR}_{off}} \cdot [pSyk] \cdot BCR^* \right) \end{cases}$$

where *[X]* represents the intracellular concentration of protein species X (Figure 3A). The single free parameter in our model is BCR^*, representing the number of constitutively activated BCRs on the cell surface. We could avoid overfitting, as all other parameters were measured or taken from the literature and assumed to be identical for all CLL and healthy B cell simulations (see Table 1).

We resolved this set of differential equations using the ode45 solver, a nonstiff ordinary differential equation solver in MATLAB. We simulated our experimental conditions:

responses of pSYK and pLYN for varied concentrations of H_2O_2 at steady state, starting from resting or fully activated states. As with our primary *ex vivo* experiments, relaxation from full H_2O_2 activation (phosphatase inhibition) permits the assessment of hysteresis within the BCR signaling pathway.

Our model established that for individual B cells, low levels of constitutive BCR activation yield a single steady state of LYN and SYK activation with minimal phosphorylation; high levels of constitutive BCR activation yield a single steady state of LYN and SYK activation with complete phosphorylation, whereas intermediate levels of constitutive BCR activation induce two stable fixed points in the (pLYN, pSYK) phase space (Figures 3B and S3B). Two stable fixed points enable bistability in phosphorylation patterns. Hence, we found that by varying only the level of constitutive BCR activation, we could transverse the phase space from dominant-monostable population behavior to dominant-bistable population behavior. Next, to match our experimental observations, we modeled the large endogenous variability in the abundances of LYN, SYK, and PTPx (e.g., SHP-1) among B cells from both CLL and healthy donors (Table 1). Such large variabilities in the expression of signaling components can be characterized by lognormal distributions with a coefficient of variation ~0.5, measured directly from single cells using flow cytometry (Figures S3C and S3D). Given these observations, we incorporated heterogeneous abundances of LYN, SYK, and PTPx proteins, and updated our dynamic model to take into account the natural phenotypic variability in isogenic populations of B cells. We typically modeled 1,000 cells with protein abundance parameters randomly chosen from the tri-variate distribution of signaling components and recorded their digital signaling output at the individual cell level (Figures S3E and S3F).

Our model successfully reproduced key aspects of the signaling responses of B cells, as documented in Figure 1. Modeled cells are bistable in their phosphorylation response to H_2O_2. Simulated activation of a population of B cells results in switch-like activation on a cell-to-cell basis (Figures 1B, 1D, and S3F). Our model reproduces the observation that higher degrees of constitutive signaling, here modeled as a larger abundance of constitutively active BCR, drives hypersensitivity to digital activation (Figures 3C, left panel, and 3D). Furthermore, simulations of this model successfully represent coupling between the hypersensitivity observation and the presence of more extreme hysteresis, observed as sustained kinase phosphorylation after H_2O_2 removal (Figures 3C, right panel, 3E, and 3F). We observe that substantial phenotypic variation can be accessed without imposing altered signaling network structures. Notably, the hysteresis ranges from 0% to 51% by altering the constitutive BCR signaling parameter BCR^*. To assess the sensitivity of our results to parameter fluctuations, we varied each parameter from 0.1 to 10x compared to the original measured value and recorded how these alterations affected the H_2O_2 EC_{50}^{up} result for SYK phosphorylation (Figure S3G). As expected, BCR clustering and the abundance of active phosphatase critically affect signaling activity within our model, while variations in catalytic rates and binding constants had a limited effect. By simulating the outcomes of LYN or SYK inhibition after stimulation, our model supports our finding that bistability and hysteresis are fully dependent on a SYK positive feedback motif (Figure S5A).

To conclude, we modeled BCR-proximal signaling using a two-equation dynamic model to account for the phosphorylation status of kinases LYN and SYK after phosphatase inhibition. We confirmed that bistability and hysteresis in BCR-proximal kinases are dominantly tuned by variations in the constitutive BCR stimulatory input, modeled as a generalized representation of altered BCR clustering. Finally, we confirmed that such phenomena are fully dependent on a proximal positive feedback motif, and each of our experimental observations can be recapitulated with a simple model of SYK-mediated feedback. These modeling efforts strengthen our hypothesis that signaling variability between B cells from healthy and CLL patients and between different CLL donors can arise purely from varied constitutive activation of the BCR without requiring genetic alterations in the downstream signaling network structure (Figure 3C). Thus, our theoretical effort encapsulates the salient features of CLL BCR dysfunction and makes testable predictions that further our understanding of CLL biology.

Crosslinking of BCR on B Cells from Healthy Individuals Phenocopies Signaling Dysfunction in CLL

Our model predicts that variability in B cell responses could stem from variable degrees of surface Ig clustering, which may be associated with the natural genomic heterogeneity in BCRs (i.e., somatic mutations in IgM during B cell development) or acquired hypermutation and auto-affinity due to the response to self or a pathogen (Dühren-von Minden et al., 2012) (Figures 3D-3F). To assess this prediction, we induced stable BCR clustering on the surface of B cells from healthy donors using a bivalent polyclonal anti-IgM antibody. We confirmed that this was sufficient to increase the responsiveness of B cells to lower concentrations of H_2O_2, and enabled hysteresis (Figures 4A and 4B). Moreover, by titrating the amount of anti-IgM crosslinking, healthy B cells could be induced to recapitulate the diversity in signaling observed in CLL B cells (Figure 4C). This confirmed our model prediction that BCR clustering can alone induce hyperresponsiveness to stimulation and hysteresis in the BCR-proximal signaling network. Further, this observation establishes that the two dynamic features, an increase in EC_{50}^{up} and a decrease in $\%\ pSYK^{+}_{hysteresis}$, are directly linked (model: Figures 3D-3F; data: Figures 4C and 4D). We found that B cells from different CLL patients similarly obey this scaling property, whereby individual leukemic clones with the most robust $\%\ pSYK^{+}_{hysteresis}$ exhibit the highest hypersensitivity to activation (model: Figure 3F; data: Figure 4D). Our theoretical model and experimental results suggest that dysfunctional signaling dynamics in CLL B cells could be phenocopied by inducing clustering of surface BCR in healthy B cells and that constitutive signaling represents a universal, tunable signaling mechanism underlying B cell activation dynamics.

Super-Resolution Microscopy Resolves BCR Clusters on the Surface of Cells and Quantifies CLL Constitutive Signaling

To understand the phenotype of surface Ig on CLL B cells, we visualized and quantified the degree of constitutive BCR clustering on the surface of B cells using super-resolution microscopy (d-STORM). B cells from CLL patients and healthy donors were stained at 4°C with a fluorescently coupled antibody against IgM, deposited on a coverslip, and imaged under total internal reflection illumination with a blink-inducing buffer (Figures S4A and

S4B) (Lee et al., 2017). d-STORM imaging of individual BCRs achieves a 15-nm resolution (Baddeley and Turner, 2005), which allowed us to quantify the total abundance of BCRs (Figure S4C) and their propensity to aggregate on the surface of B cells by measuring the fraction of individual BCRs that lay within this minimal binding radius of another BCR at steady state (Figures 4E and S4B). Compared to 31% ± 5% of BCRs on the surface of healthy donor derived B cells (n = 18), 58% ± 3% of BCRs on the surface of CLL B cells (n = 64) belong to a cluster ($p < 0.0001$ by Student's t test; Figures 4F, S4B, and S4D). As predicted by our model, there is a strong correlation between the fraction of clustered BCRs (as a measure of constitutive BCR activation) and stimulation hypersensitivity and hysteretic signaling behavior induced by transient phosphatase inhibition (Figures 4G, $p < 0.01$, and 4H, $p < 0.01$). As a positive control, we crosslinked BCRs on healthy donor B cells at 37°C with a bivalent anti-IgM antibody before staining cells at 4°C. Crosslinked healthy B cells demonstrated enhanced clustering of BCRs, which is on par with the degree of clustering observed in CLL B cells (n = 12) ($p < 10^{-4}$ compared to uncrosslinked healthy B cells by Student's t test; Figures 4E and 4F). Again, enhanced BCR clustering on healthy B cells correlated with hypersensitivity and hysteresis in the signaling patterns after phosphatase inhibition (Figures 4G and 4H). Thus, the percentage of BCRs engaged in a cluster can be considered an experimental estimate of the level of constitutive activation of a cell, which drives differential responsiveness to phosphatase inhibition.

Finally, using the predicted scaling between BCR constitutive signaling and $\%\ pSYK^{+}_{hysteresis}$, we applied our dynamic model to the $\%\ pSYK^{+}_{hysteresis}$ measured from patient-derived B cells and generated calibrated predictions of the degree of BCR clustering on the surface of cells (Figure 4I). Super-resolution imaging of the BCR membrane phenotype strongly confirmed this model prediction and established our single-cell assay of BCR signaling dynamics as sufficient to estimate the unique degrees of constitutive activation for each leukemic clone.

A Biophysical Assay Demonstrates the Propensity for BCRs to Cluster on the Surface of CLL B Cells

We confirmed our observation of BCR membrane clustering in CLL clones with a custom qualitative biophysical assay (Figure S4E). We reasoned that enhanced clustering on the surface of CLL B cells may rely on intrinsic auto-affinity between BCRs or affinity to another feature on the cellular surface. We collected plasma from whole-blood isolates from CLL patients and healthy donors and coated magnetic beads with soluble IgM/IgG. Next, we tested whether the soluble Ig from both neoplastic and healthy cells exhibited affinity toward a polyclonal pool of B cells derived from healthy donors (Figures S4E and S4F). We used flow cytometry to assess the relative binding affinity between Ig-coated beads and B cells, as cells bound to beads could be readily distinguished from unbound cells by light-scattering properties. By costaining with surface markers, we could measure the "depletion" of B cells from the unbound cellular pool, providing a proxy for affinity between the Ig captured on the beads and healthy B cells. We calibrated our measurements using negative control beads coated with mouse gamma globulin, which was expected to exhibit negligible affinity toward human B cells and anti-IgM coated beads, which we expected to strongly bind to the surface of B cells. As expected, anti-IgM coated beads had the capacity to selectively deplete B cells

from the unbound cellular fraction, while mouse gamma globulin-coated beads exhibited negligible B cell binding (Figures S4F and S4G). Similarly, we observed that secreted Ig isolated from healthy plasma exhibited little affinity for healthy B cells. In contrast, beads coated with serum Ig isolated from representative sets of CLL patients bound to the surface of B cells at high affinity relative to healthy donor-derived Ig, at similar rates in our assay to anti-IgM bivalent antibodies, and resulted in the near-complete depletion of B cells from the unbound cellular fraction ($p < 0.001$; Figures S4F and S4G). Such auto-reactive binding capacity, combined with the bivalency of surface Ig, correlates qualitatively with enhanced IgM clusters on the surface of CLL B cells, as observed by super-resolution microscopy (Figure 4F). Notably, we found that this unique property of CLL-derived Ig is not patient specific. Ig derived from a given CLL patient has the capacity to bind non-specifically to the surface of any B cell tested, including other CLL leukemic clones and healthy donor B cells. Hence, the antigen driving Ig clustering on the surface of CLL B cells may be due to mutations in a constant region of Ig or it may reflect affinity to other surface proteins. Clustering of surface Ig is thus ubiquitous, variable, and sufficient to account for the magnitude of proximal-BCR signaling that is characteristic of primary CLL B cells.

Cell-to-Cell Variability Analysis Validates the Role of Phosphatases in Defining the Threshold for BCR Activation

Our understanding of signaling hypersensitivity within CLL B cells is supported by our computational model of the early events in signal transduction at and downstream of BCR clustering. To further our understanding of signaling dysregulation in CLL, we applied cell-to-cell variability analysis (CCVA) (Cotari et al., 2013a, 2013b) to quantify how variability in B cell signaling relates to the abundance of phosphatases at the single-cell level (Figure 5A). Briefly, this technique allows us to leverage the diversity in protein abundance within isogenic cell populations to learn regulatory mechanisms of signaling responses. Here, we apply this method to better understand how altered negative regulators may affect kinase activation. We stimulated PBMCs with varied doses of H_2O_2 for 4 min and measured the signaling response using phospho-flow cytometry. We co-stained cells for pPLCγ2 and SHP-1 (i.e., PTPN6) abundance. SHP-1 is a phosphatase of critical relevance in antigenic signaling responses in lymphocytes and, crucially, the phosphatase responsible for mediating signaling repression via CD5 upregulation in lymphocytes and thus relevant for CLL signaling dynamics (Feinerman et al., 2008; Khalil et al., 2012). A coarse-grained approach to CCVA is illustrated in Figures 5B and 5C, in which the distribution of SHP-1 abundance in a B cell population is partitioned into discrete subpopulations, termed "SHP-1^{low}," "SHP-1^{int}," and "SHP-1^{high}." Each B cell subset displays unique and reproducible deviations in their signaling responses measured by pPLCγ2, wherein cells with high concentrations of SHP-1 are hyporesponsive to H_2O_2 stimulation, as observed by fewer pPLC$\gamma 2^+$ cells (red lines, Figure 5C). We applied CCVA to the distribution of SHP-1 abundance. We binned our single-cell data for varied levels of SHP-1 and measured the amount of phosphorylated PLCγ2 within each subpopulation for increasing concentrations of H_2O_2 (Figure 5D). This analysis permits B cell stimulation to be analyzed as a "dose response" of phosphatase abundance, and B cells from distinct donors can be directly compared within similarly binned SHP-1 (Figure 5E). These experimental measurements confirmed a prediction from our model (Figures 5F, S5B, and S5C): increasing levels of

SHP-1 correlate with blunted activation within populations of CLL or healthy B cells. However, we do not And that changes in the abundance of SHP-1 between healthy and CLL B cells are responsible for disease-specific differences in sensitivity to phosphatase inhibition. Furthermore, model simulations do not support alterations in phosphatase functionality, such as mutations in dominant BCR-proximal phosphatases, or upregulation or downregulation at the cell membrane, to enable hysteretic behaviors as we observe in our data (Figures S5C and S5D). This further validated our model and emphasized how phenotypic variability within isogenic populations of tumor cells can result from heterogeneous abundances of signaling regulators.

Clinical Correlates of BCR Dysfunction in CLL and Other B Cell Neoplasms

The reported measurements of signaling dysfunction capture large and reproducible variability between B cells from CLL patients and healthy counterparts, and subsequent investigation revealed that signaling alteration is potentially linked to a prior response to an antigen or a pseudo-antigen. As the typical impact of BCR stimulation and downstream PLCγ2 phosphorylation and PI3K activation is enhanced cell survival and proliferation, we examined whether BCR signaling dynamics were related to clinical phenotypes. We measured the degree of hysteresis in SYK phosphorylation in B cells from 91 patients afflicted with B cell leukemias and lymphomas of a diverse nature (Table S1). In this expanded cohort, we again found that the $\% \, pSYK^{+}_{hysteresis}$ is significantly higher in B cells from CLL patients compared to healthy donors ($p < 0.01$; Figure 6A). We similarly observed elevated and variable hysteresis among B cells from patients with mantle cell lymphoma (MCL); a notable commonality between these lymphoma subtypes is the surface expression of CD5 on B cells, and each exhibit a similar clinical presentation ($p < 0.05$; Figures 6A and S6A) (Puente et al., 2018). Hysteresis was negligible (within the healthy donor range) in B cells from patients with follicular lymphoma (FL) and marginal zone lymphoma (MZL) (Figure 6A). Within the cohort of CLL patients, we also found that $\% \, pSYK^{+}_{hysteresis}$ was associated with the severity of the disease, as determined retrospectively by estimating the clinical need of treatment at the time of blood draw ($p < 0.0038$; Figures 6B and S6B) or the probability of remaining progression free ($p < 0.0040$; Figure 6C). It has been previously proposed that unmutated heavy-chain immunoglobulin variable regions in clonal CLL B cells are more responsive to antigenic stimulation and are associated with poorer prognoses (Damle et al., 1999; Hamblin et al., 1999; Oscier et al., 2002). However, in the cohort we tested, we did not find a significant association between the BCR mutation status and the magnitude of $\% \, pSYK^{+}_{hysteresis}$ (Figure S6C). In addition, a longitudinal study of patients whose CLL required treatment (“Progressors”) versus patients whose CLL could remain untreated and under observation (“Non Progressors”) yielded a marked difference in the dynamics of $\% \, pSYK^{+}_{hysteresis}$ ($p < 0.0022$; Figure 6D). We found that independent of initial BCR signaling status, B cells from Progressors increased in their $\% \, pSYK^{+}_{hysteresis}$ over time, while B cells from the Non Progressors remained stable.

Our findings open up new opportunities in clinical immunology, whereby assessing the response of leukemic clones to phosphatase inhibition could be used to infer the degree of

BCR clustering and predict clinical presentation (Figure 6E). The origin and functional significance of the dichotomy of disease progression reflected in BCR hyperresponsiveness will require additional study to assess its relevance in the treatment of CLL.

DISCUSSION

In this study, we used a combination of single-cell phospho-profiling and computational modeling to uncover signaling dysregulation within B cells in primary tumors from CLL patients. This methodology enabled us to quantitatively assess aberrant signaling, model and validate specific molecular drivers of signaling dysfunction, and conclude that increased constitutive activation of the BCR signalosome differentiates CLL B cells from their healthy counterparts. Our data support this dynamic phenotype as a hallmark of CLL pathobiology, connect constitutive levels of BCR activation to variability in the behavior of single cells, and strongly correlate with overall clinical outcome.

Concurrently, our study demonstrates the strength of systems immunology, in particular, simple mathematical modeling, to quantitatively dissect the pathophysiology of tumor cells. Through dynamic modeling, we assessed the impact of diverse mutational backgrounds with unbiased filtering and were able to pinpoint important “nodes” of dysregulation across heterogeneous patient samples. In our study of CLL, we demonstrated that the interplay between constitutive signaling through BCR clustering and a positive feedback in the early signaling events was sufficient to account for the variability of responsiveness in the BCR signaling pathway.

While other groups have attempted more comprehensive and systematic modeling of cellular function (Karr et al., 2012), our study highlights the degree of biochemical precision that is required to capture functionally relevant aspects to leukocyte physiology, which can be achieved only by limiting signaling networks to those components or motifs that directly filter and propagate relevant stimuli. In the present case of CLL, a small increase in constitutive BCR signaling led to great changes in signal responsiveness after phosphatase inhibition. Recent results from the field of network biology have demonstrated that cell responsiveness may be fully determined by a few “critical modes” (Machta et al., 2013); instead of requiring a full accounting of all of the molecular events, systems immunologists can focus on a few critical modes whose dynamics encapsulate most relevant biological functions. In CLL, subclonal evolution occurs within a population of B cells that maintains clonality within the BCR (Landau et al., 2013). We therefore surmise that the BCR-driven hyperresponsiveness of CLL B cells may be the dominant mode onto which additional oncogenic transformations become fixed (e.g., p53 mutation, chromosomal deletion; Chiorazzi et al., 2005).

Our findings also augment the recent insights about the role of the BCR in CLL pathobiology, emerging from genomic (Agathangelidis et al., 2012), functional (Dühren-von Minden et al., 2012), and mouse genetic modeling studies (Chen et al., 2015; Dühren-von Minden et al., 2012; Iacovelli et al., 2015). In particular, our method demonstrates that the cell-autonomous antigen-independent signaling response associated with CLL is highly variable and specific for each individual CLL B cell clone. Our data and model imply that

increased BCR clustering (evident in CLL B cells) is a perturbed cell state along the natural continuum of healthy B cell biology—an extreme and malignant phenotype arising due to signaling dynamics (proximal positive feedback engendering hysteresis and bistability) as opposed to a concrete, singular mutational event. This observation potentially puts to rest the long-unresolved finding of dysfunctional kinase activation and phosphorylation in CLL B cells without mutational “hits” in these pathways. Moreover, our observation opens up the possibility that other B cell neoplasms, auto-inflammatory conditions, or even natural benchmarks along B cell development rely on tunable scaling between locally perturbed membrane clustering and the capacity for cell-autonomous sustained activation (Minguet et al., 2017). Finally, our methodology may provide an additional clinical tool to stratify CLL patients by severity according to the degree of constitutive signaling in their B cell clone. Future studies will be needed to couple our quantitative assessment of BCR dysfunction with compensatory mechanisms and downstream mutations to lead to better classification, diagnosis, and treatment of CLL on a personalized basis.

STAR★METHODS

LEAD CONTACT AND MATERIALS AVAILABILITY

Further information and requests for resources and reagents should be directed to and will be fulfilled by the Lead Contact, Gregoire Altan-Bonnet (gregoire.altan-bonnet@nih.gov).

EXPERIMENTAL MODEL AND SUBJECT DETAILS

Peripheral blood samples were obtained from 57 CLL patients, 14 healthy donors, 28 Mantle Cell Lymphoma (MCL) patients, 2 Follicular Lymphoma (FL) patients, and 4 Marginal Zone Lymphoma (MZL) patients. Samples were collected from Memorial Sloan Kettering Cancer Center. All donors consented for PBMCs to be used for research purposes, in accordance with the Declaration of Helsinki and approval by the Memorial Sloan Kettering Cancer Center institutional review board. Patients were not selected on the basis of disease characteristics or treatment history, nor were they treated uniformly under a specific clinical trial. The median age of CLL patients was 71, range: 44-91. Details on disease attributes can be found in Table S1. 37% of CLL patients identified as female, and 50% of healthy donors identified as female. In the study described in Figure 6A, the gender of the donor was not predictive of $\%\ pSYK^{+}_{hysteresis}$: female: 66.5 ± 7.3, male: 61.5 ± 5.3, p = 0.57 by Student’s t test.

METHOD DETAILS

Cell Preparation and Perturbation—Peripheral blood mononuclear cells (PBMCs) were isolated using density gradient separation (Ficoll-Paque Plus; GE Healthcare) and frozen within 6 hours of collection. Cells were thawed, rested and stimulated as previously described (Irish et al., 2004; Khalil et al., 2012; Palomba et al., 2014). Briefly: frozen cells were thawed by gentle resuspension in RPMI 1640 media supplemented with 10% fetal bovine serum (FBS, Thermo Fisher Scientific), and plated at 10^7 cells/mL. Cells were rested for 2 hours at 37°C, and stimulated with a range of doses of hydrogen peroxide (H_2O_2, Sigma) for 4 minutes at 37°C. For assessment of sensitivity to stimulation from rest, cells

were immediately fixed after 4-minute stimulation by addition of pre-warmed (37°C) paraformaldehyde (PFA, BD Biosciences). For assessment of hysteresis (phosphorylated kinase activity following removal of stimulus), instead of fixing cells following 4-minute stimulation, cells were placed in either RPMI with 10% FBS media alone, or in addition to a range of concentrations of H_2O_2. Doses for H_2O_2 stimulation and timing post-stimulation is specified in figures or figure captions. Cells were stimulated with polyclonal Goat anti-Human anti-IgM F(ab')2 (Invitrogen) by adding 1 μg/mL anti-IgM to cells at 37°C for 4 minutes in parallel with H_2O_2 stimulation. Alternative concentrations of anti-IgM stimulation are noted in figures or figure captions. Pervanadate (Sigma) was prepared for cell stimulation as described (Huyer et al., 1997), and cells were stimulated identically to H_2O_2 stimulation. The inhibitors of kinase signaling, PP2 (Sigma) and R406 (Santa Cruz Biotech), and vehicle-control DMSO, were applied to cellular media at concentrations and timing as noted in figure captions.

Phospho-Flow Cytometry—Antibodies with the following specificities were purchased from BD Biosciences: pPLCγ2 (Alexa Fluor 488, pY759), pSYK (PE, pY348), pLCK/pLYN (Alexa Fluor 647, pY505). Phosphatase abundance was estimated by SHP-1 antibody (Santa Cruz Biotechnology). Detection of PBMC subsets was achieved with Pacific Blue-conjugated anti-CD3 (clone UCHT1) and PerCPCy5.5 conjugated anti-CD20 (clone H1), and CLL circulating tumor was confirmed for CD5 positivity with PE-Cy7-conjugated anti-CD5 (clone L17F12, all BD Biosciences). Intracellular reactive oxygen species was measured under resting and H_2O_2-stimulated conditions using 2′,7'-dichlorofluorescin diacetate (DCFDA) (Abcam). For assessment of intracellular species, cells were permeabilized following fixation with PFA with cold methanol at −20°C for 10 minutes. Intracellular staining was carried out at 4°C in PBS + 2% FBS. Cells were washed twice with PBS + 2% FBS and analyzed on an LSRII cytometer (BD Biosciences). Analysis was carried out using FlowJo software (TreeStar), Prism (Graphpad), and with custom tools written in R statistical computing language (R project) and MATLAB (Mathworks). Code is available upon request.

Bead Affinity Assay—To develop a qualitative test to assess the specificity of secreted Ig, we modified the protocol presented in Coelho et al. (Figure S4E) (Coelho et al., 2013). Magnetic Protein A coated beads (Dynabeads, Life Technologies) were saturated with Ig from plasma frozen in parallel to above PBMC freezing protocol, according to the manufacturer's instructions. This permitted generation of beads coated with specific secreted Ig from different CLL and healthy donors. Mouse gamma globulin (Jackson ImmunoChemicals) and purified recombinant human IgM (Sigma) were used as negative controls, for which affinity for molecules on B cell membranes is negligible and non-specific. Conversely, beads coated with Goat anti-Human anti-IgM (Invitrogen) were used as a positive control for bead-Ig-B cell binding. Beads were incubated with mouse gamma globulin to block any unoccupied protein A binding sites. All incubations were carried out while rotating at room temperature for 2 hours. Each bead sample was verified by flow cytometry for intended loading and full surface saturation (data not shown). Healthy PBMCs were incubated with beads at a ratio of 10:1 beads:cells for 2 hours at 37°C, and fixed using PFA at a final concentration of 1.6%, stained for surface proteins CD20 and CD3 as

described above, and analyzed using an LSRII cytometer (BD Biosciences). We utilized altered light scattering in bead-bound cells (FSC/SSC) to compare cellular fractions in bead-binding (therefore, Ig-binding) and unbound populations (Figure S4F).

PALM/dSTORM Superresolution Microscopy—Frozen PBMCs were thawed and washed in RPMI with 10% FBS and incubated at 37°C for 2 hours. Cells were stained with Goat anti-Human anti-IgM F(ab')2 (Invitrogen), followed by Donkey anti-Goat A647 (Jackson). Cells were washed in PBS and loaded onto a coverslip coated with Mouse anti-Human HLA-DP (Abd Serotec). Finally, cells were affixed onto the coverslip with 4% PFA. Cells were stained with excess antibody and maintained on ice for the entire staining and mounting protocol to minimize antibody-induced BCR crosslinking. This protocol was modified for the positive, cross-linked control by staining with anti-IgM at 37°C.

An oxygen-scavenging PBS solution (10mM NaCl, 0.5mg/ml glucose oxidase, 40 g/ml catalase, 2% glucose and 10mM MEA) was used for imaging. dSTORM images were obtained on a Zeiss ELYRA PS.1 system (Carl Zeiss, USA). Images were acquired with a Plan-Apochromat 100x/1.46 oil immersion objective and an Andor iXon 885 EMCCD camera. 20,000 images were acquired per sample with an exposure time of 33 ms. We acquired data on the surface BCR cluster phenotype from 5 CLL patients (#046: 23 cells, #030: 10 cells, #016: 9 cells, #037: 13 cells, #022: 9 cells), 2 healthy donors (#092: 7 cells, #093 11 cells), and 1 positive control healthy donor with anti-IgM crosslinking (#092: 12 cells).

Raw images were reconstructed and analyzed with ZEN software (Carl Zeiss, USA) and R package spatstat (Baddeley et al., 2015). Nearest neighbor calculations were applied to quantify BCR-BCR interactions, and the fraction of BCR/cell in a cluster was defined as 1 - p(monomer), where a monomer was defined as any BCR with no other BCRs identified within a 15 nm radius.

QUANTIFICATION AND STATISTICAL ANALYSIS

All statistical details can be found in the figure legends, including statistical tests, p values (if reported), and exact values of n. p values less than 0.05 were considered significant. Comparison of EC_{50}^{up} and $\%\ pSYK_{hysteresis}^{+}$ values between disease groups was calculated by two-tailed Student's t test or one-way ANOVA using Prism software (noted in figure legends). EC_{50}^{up} calculations were completed using Prism by fitting a Hill equation to the dose response curve enabling a variable hill coefficient. Ordinary differential equation modeling was completed using the ode45 solver in MATLAB (Mathworks). Code available upon request.

Supplementary Material

Refer to Web version on PubMed Central for supplementary material.

ACKNOWLEDGMENTS

We thank members of the ImmunoDynamics Group, Jackie Bromberg, Olivier Elemento, and Omar Abdel Wahab for useful comments and discussions. This work was supported by NIH grant U54 CA148967 (to C.G.K.Z., M.L.P., K.P., A.O.-Y., M.R.M.v.d.B., and G.A.-B.); the Geoffrey Beene Cancer Center (to J.K. and G.A.-B.); Cycle for Survival (to J.K., K.V.A., M.L.P., and G.A.-B.); National Institute of General Medical Sciences (NIGMS) grant T32GM007753 (to C.G.K.Z.); and the intramural research programs of the National Heart, Lung, and Blood Institute (NHLBI) (to N.A.-B.) and the Center for Cancer Research, National Cancer Institute (NCI), NIH (to G.A.-B.).

REFERENCES

Agathangelidis A, Darzentas N, Hadzidimitriou A, Brochet X, Murray F, Yan XJ, Davis Z, van Gastel-Mol EJ, Tresoldi C, Chu CC, et al. (2012). Stereotyped B-cell receptors in one-third of chronic lymphocytic leukemia: a molecular classification with implications for targeted therapies. Blood 119, 4467–4475. [PubMed: 22415752]

Altan-Bonnet G, and Germain RN (2005). Modeling T cell antigen discrimination based on feedback control of digital ERK responses. PLoS Biol. 3, e356. [PubMed: 16231973]

Baddeley A, and Turner R (2005). spatstat: An R Package for Analyzing Spatial Point Patterns. J Stat Softw. 12, 1–42.

Baddeley A, Rubak E, and Turner R(2015). Spatial Point Patterns: Methodology and Applications with R (Chapman and Hall/CRC Press).

Barua D, Hlavacek WS, and Lipniacki T (2012).A computational model for early events in B cell antigen receptor signaling: analysis of the roles of Lyn and Fyn. J. Immunol 189, 646–658. [PubMed: 22711887]

Binder M, Müller F, Frick M, Wehr C, Simon F, Leistler B, Veelken H, Mertelsmann R, and Trepel M (2013). CLL B-cell receptors can recognize themselves: alternative epitopes and structural clues for autostimulatory mechanisms in CLL. Blood 121, 239–241. [PubMed: 23287626]

Chen Z, Shojaee S, Buchner M, Geng H, Lee JW, Klemm L, Titz B, Graeber TG, Park E, Tan YX, et al. (2015). Signalling thresholds and negative B-cell selection in acute lymphoblastic leukaemia. Nature 521, 357–361. [PubMed: 25799995]

Chiorazzi N, Rai KR, and Ferrarini M (2005). Chronic lymphocytic leukemia. N. Engl. J. Med 352, 804–815. [PubMed: 15728813]

Coelho V, Krysov S, Steele A, Sanchez Hidalgo M, Johnson PW, Chana PS, Packham G, Stevenson FK, and Forconi F (2013). Identification in CLL of circulating intraclonal subgroups with varying B-cell receptor expression and function. Blood 122, 2664–2672. [PubMed: 23954894]

Cotari JW, Voisinne G, and Altan-Bonnet G (2013a). Diversity training for signal transduction: leveraging cell-to-cell variability to dissect cellular signaling, differentiation and death. Curr. Opin. Biotechnol 24, 760–766. [PubMed: 23747193]

Cotari JW, Voisinne G, Dar OE, Karabacak V, and Altan-Bonnet G (2013b). Cell-to-cell variability analysis dissects the plasticity of signaling of common γ chain cytokines in T cells. Sci. Signal 6, ra17. [PubMed: 23482665]

Damle RN, Wasil T, Fais F, Ghiotto F, Valetto A, Allen SL, Buchbinder A, Budman D, Dittmar K, Kolitz J, et al. (1999). Ig V gene mutation status and CD38 expression as novel prognostic indicators in chronic lymphocytic leukemia. Blood 94, 1840–1847. [PubMed: 10477712]

Damle RN, Ghiotto F, Valetto A, Albesiano E, Fais F, Yan XJ, Sison CP, Allen SL, Kolitz J, Schulman P, et al. (2002). B-cell chronic lymphocytic leukemia cells express a surface membrane phenotype of activated, antigen-experienced B lymphocytes. Blood 99, 4087–4093. [PubMed: 12010811]

Das J, Ho M, Zikherman J, Govern C, Yang M, Weiss A, Chakraborty AK, and Roose JP (2009). Digital signaling and hysteresis characterize ras activation in lymphoid cells. Cell 136, 337–351. [PubMed: 19167334]

Davis RE, Ngo VN, Lenz G, Tolar P, Young RM, Romesser PB, Kohlhammer H, Lamy L, Zhao H, Yang Y, et al. (2010). Chronic active B-cell-receptor signalling in diffuse large B-cell lymphoma. Nature 463, 88–92. [PubMed: 20054396]

Döhner H, Stilgenbauer S, Benner A, Leupolt E, Kröber A, Bullinger L, Döhner K, Bentz M, and Lichter P (2000). Genomic aberrations and survival in chronic lymphocytic leukemia. N. Engl. J. Med 343, 1910–1916. [PubMed: 11136261]

Dühren-von Minden M, Übelhart R, Schneider D, Wossning T, Bach MP, Buchner M, Hofmann D, Surova E, Follo M, Köhler F, et al. (2012). Chronic lymphocytic leukaemia is driven by antigen-independent cell-autonomous signalling. Nature 489, 309–312. [PubMed: 22885698]

Feinerman O, Veiga J, Dorfman JR, Germain RN, and Altan-Bonnet G (2008). Variability and robustness in T cell activation from regulated heterogeneity in protein levels. Science 321, 1081–1084. [PubMed: 18719282]

Ferrell JE Jr., and Machleder EM (1998). The biochemical basis of an all-or-none cell fate switch in Xenopus oocytes. Science 280, 895–898. [PubMed: 9572732]

Gomes de Castro MA, Wildhagen H, Sograte-Idrissi S, Hitzing C, Binder M, Trepel M, Engels N, and Opazo F (2019). Differential organization of tonic and chronic B cell antigen receptors in the plasma membrane. Nat. Commun 10, 820. [PubMed: 30778055]

Gunawardena J (2014). Models in biology: 'accurate descriptions of our pathetic thinking.'. BMC Biol. 12, 29. [PubMed: 24886484]

Hamblin TJ, Davis Z, Gardiner A, Oscier DG, and Stevenson FK (1999). Unmutated Ig V(H) genes are associated with a more aggressive form of chronic lymphocytic leukemia. Blood 94, 1848–1854. [PubMed: 10477713]

Harwood NE, and Batista FD (2010). Early events in B cell activation. Annu. Rev. Immunol 28, 185–210. [PubMed: 20192804]

Hoogeboom R, van Kessel KP, Hochstenbach F, Wormhoudt TA, Reinten RJ, Wagner K, Kater AP, Guikema JE, Bende RJ, and van Noesel CJ (2013). A mutated B cell chronic lymphocytic leukemia subset that recognizes and responds to fungi. J. Exp. Med 210, 59–70. [PubMed: 23296468]

Huyer G, Liu S, Kelly J, Moffat J, Payette P, Kennedy B, Tsaprailis G, Gresser MJ, and Ramachandran C (1997). Mechanism of inhibition of protein-tyrosine phosphatases by vanadate and pervanadate. J. Biol. Chem 272, 843–851. [PubMed: 8995372]

Iacovelli S, Hug E, Bennardo S, Duehren-von Minden M, Gobessi S, Rinaldi A, Suljagic M, Bilbao D, Bolasco G, Eckl-Dorna J, et al. (2015). Two types of BCR interactions are positively selected during leukemia development in the Eμ-TCL1 transgenic mouse model of CLL. Blood 125, 1578–1588. [PubMed: 25564405]

Irish JM, Hovland R, Krutzik PO, Perez OD, Bruserud Ø, Gjertsen BT, and Nolan GP (2004). Single cell profiling of potentiated phospho-protein networks in cancer cells. Cell 118, 217–228. [PubMed: 15260991]

Karr JR, Sanghvi JC, Macklin DN, Gutschow MV, Jacobs JM, Bolival B Jr., Assad-Garcia N, Glass JI, and Covert MW (2012). A whole-cell computational model predicts phenotype from genotype. Cell 150, 389–401. [PubMed: 22817898]

Ketchum C, Miller H, Song W, and Upadhyaya A (2014). Ligand mobility regulates B cell receptor clustering and signaling activation. Biophys. J 106, 26–36. [PubMed: 24411234]

Khalil AM, Cambier JC, and Shlomchik MJ (2012). B cell receptor signal transduction in the GC is short-circuited by high phosphatase activity. Science 336, 1178–1181. [PubMed: 22555432]

Kläsener K, Maity PC, Hobeika E, Yang J, and Reth M (2014). B cell activation involves nanoscale receptor reorganizations and inside-out signaling by Syk. eLife 3, e02069. [PubMed: 24963139]

Klein U, Tu Y, Stolovitzky GA, Mattioli M, Cattoretti G, Husson H, Freedman A, Inghirami G, Cro L, Baldini L, et al. (2001). Gene expression profiling of B cell chronic lymphocytic leukemia reveals a homogeneous phenotype related to memory B cells. J. Exp. Med 194, 1625–1638. [PubMed: 11733577]

Krishnaswamy S, Spitzer MH, Mingueneau M, Bendall SC, Litvin O, Stone E, Pe'er D, and Nolan GP (2014). Systems biology. Conditional density-based analysis of T cell signaling in single-cell data. Science 346, 1250689. [PubMed: 25342659]

Landau DA, Carter SL, Stojanov P, McKenna A, Stevenson K, Lawrence MS, Sougnez C, Stewart C, Sivachenko A, Wang L, et al. (2013). Evolution and impact of subclonal mutations in chronic lymphocytic leukemia. Cell 152, 714–726. [PubMed: 23415222]

Lee J, Sengupta P, Brzostowski J, Lippincott-Schwartz J, and Pierce SK (2017). The nanoscale spatial organization of B-cell receptors on immunoglobulin M- and G-expressing human B-cells. Mol. Biol. Cell 28, 511–523. [PubMed: 27974642]

Machta BB, Chachra R, Transtrum MK, and Sethna JP (2013). Parameter space compression underlies emergent theories and predictive models. Science 342, 604–607. [PubMed: 24179222]

Minguet S, Kläsener K, Schaffer AM, Fiala GJ, Osteso-Ibánez T, Raute K, Navarro-Lérida I, Hartl FA, Seidl M, Reth M, and Del Pozo MA (2017). Caveolin-1-dependent nanoscale organization of the BCR regulates B cell tolerance. Nat. Immunol 18, 1150–1159. [PubMed: 28805811]

Minici C, Gounari M, Übelhart R, Scarfò L, Dühren-von Minden M, Schneider D, Tasdogan A, Alkhatib A, Agathangelidis A, Ntoufa S, et al. (2017). Distinct homotypic B-cell receptor interactions shape the outcome of chronic lymphocytic leukaemia. Nat. Commun 8, 15746. [PubMed: 28598442]

Mukherjee S, Zhu J, Zikherman J, Parameswaran R, Kadlecek TA, Wang Q, Au-Yeung B, Ploegh H, Kuriyan J, Das J, and Weiss A (2013). Monovalent and multivalent ligation of the B cell receptor exhibit differential dependence upon Syk and Src family kinases. Sci. Signal 6, ra1. [PubMed: 23281368]

Nadeu F, Delgado J, Royo C, Baumann T, Stankovic T, Pinyol M, Jares P, Navarro A, Martín-García D, Beà S, et al. (2016). Clinical impact of clonal and subclonal TP53, SF3B1, BIRC3, NOTCH1, and ATM mutations in chronic lymphocytic leukemia. Blood 127, 2122–2130. [PubMed: 26837699]

Oscier DG, Gardiner AC, Mould SJ, Glide S, Davis ZA, Ibbotson RE, Corcoran MM, Chapman RM, Thomas PW, Copplestone JA, et al. (2002). Multivariate analysis of prognostic factors in CLL: clinical stage, IGVH gene mutational status, and loss or mutation of the p53 gene are independent prognostic factors. Blood 100, 1177–1184. [PubMed: 12149195]

Palomba ML, Piersanti K, Ziegler CG, Decker H, Cotari JW, Bantilan K, Rijo I, Gardner JR, Heaney M, Bemis D, et al. (2014). Multidimensional single-cell analysis of BCR signaling reveals proximal activation defect as a hallmark of chronic lymphocytic leukemia B cells. PLoS One 9, e79987. [PubMed: 24489640]

Puente XS, Jares P, and Campo E (2018). Chronic lymphocytic leukemia and mantle cell lymphoma: crossroads of genetic and microenvironment interactions. Blood 131, 2283–2296. [PubMed: 29666114]

Spencer SL, Gaudet S, Albeck JG, Burke JM, and Sorger PK (2009). Non-genetic origins of cell-to-cell variability in TRAIL-induced apoptosis. Nature 459, 428–432. [PubMed: 19363473]

Tsang E, Giannetti AM, Shaw D, Dinh M, Tse JK, Gandhi S, Ho H, Wang S, Papp E, and Bradshaw JM (2008). Molecular mechanism of the Syk activation switch. J Biol Chem. 283, 32650–32659. [PubMed: 18818202]

Tsourkas PK, Baumgarth N, Simon SI, and Raychaudhuri S (2007). Mechanisms of B-cell synapse formation predicted by Monte Carlo simulation. Biophys J. 92, 4196–4208. [PubMed: 17384077]

Vogel RM, Erez A, and Altan-Bonnet G (2016). Dichotomy of cellular inhibition by small-molecule inhibitors revealed by single-cell analysis. Nat. Commun 7, 12428. [PubMed: 27687249]

Yang J, and Reth M (2010a). The dissociation activation model of B cell antigen receptor triggering. FEBS Lett. 584, 4872–4877. [PubMed: 20920502]

Yang J, and Reth M (2010b). Oligomeric organization of the B-cell antigen receptor on resting cells. Nature 467, 465–469. [PubMed: 20818374]

Zhang Z, Zemlin M, Wang YH, Munfus D, Huye LE, Findley HW, Bridges SL, Roth DB, Burrows PD, and Cooper MD (2003). Contribution of Vh gene replacement to the primary B cell repertoire. Immunity 19, 21–31. [PubMed: 12871636]

Highlights

- Bistability and hysteresis are dynamically controlled by BCR clustering
- Mathematical modeling predicts enhanced BCR clustering in CLL
- Super-resolution microscopy confirms CLL BCRs auto-aggregate at steady state
- CLL B cell signaling varies between patients and predicts disease severity

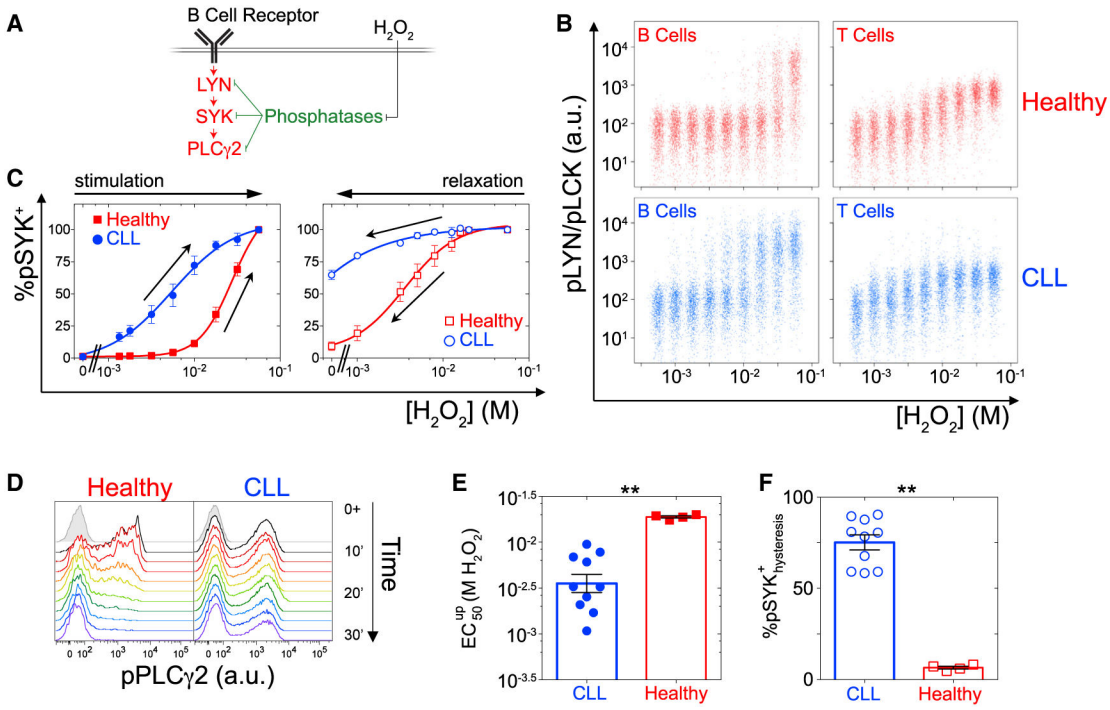

Figure 1. Phospho-Flow Cytometry to Characterize the Proximal Defects in BCR Signaling in CLL

(A) Schematic of main components of the BCR signaling pathway under investigation.

(B) Phospho-flow cytometry of B cells and T cells for pLYN and pLCK (respectively, using a pleiotropic antibody) after a 4-min exposure to H_2O_2. Representative plot from one healthy donor (red, top row) and one CLL donor (blue, bottom row). Lymphocytes were gated on B cells ($CD3^{-}CD20^{+}$, left) or T cells ($CD3^{+}CD20^{-}$, right). Individual cells are plotted for each $[H_2O_2]$. a.u., amplitude units.

(C) $\%pSYK^{+}$ B cells from CLL patients (n = 4, blue) and healthy donors (n = 2, red) following exposure to increasing ("stimulation," left) or decreasing ("relaxation," right) concentrations of H_2O_2. See STAR Methods for protocol details. Open icons denote relaxation following stimulation; filled icons denote stimulation from rest.

(D) Histograms of pPLCγ2 in B cells following stimulation with H_2O_2 and return to stimulation-free media (starting at 0+ curve, black line). Gray histogram, unstimulated cells. Left, representative healthy donor; right, representative CLL donor.

(E) The half-maximal H_2O_2 concentration (EC_{50}^{up}) for SYK phosphorylation from rest among B cells from CLL patients (n = 10) and healthy donors (n = 4). **p < 0.01 by Student's t test.

(F) $\%pSYK^{+}$ B cells following H_2O_2 activation and return to stimulation-free media ($\%\ pSYK^{+}_{hysteresis}$) from CLL (blue, n = 10) and healthy (red, n = 4) donors. Steady state is achieved after 30 min of incubation in stimulation-free media. **p < 0.01 by Student's t test. The data are represented as means ± SEMs. See also Figure S1.

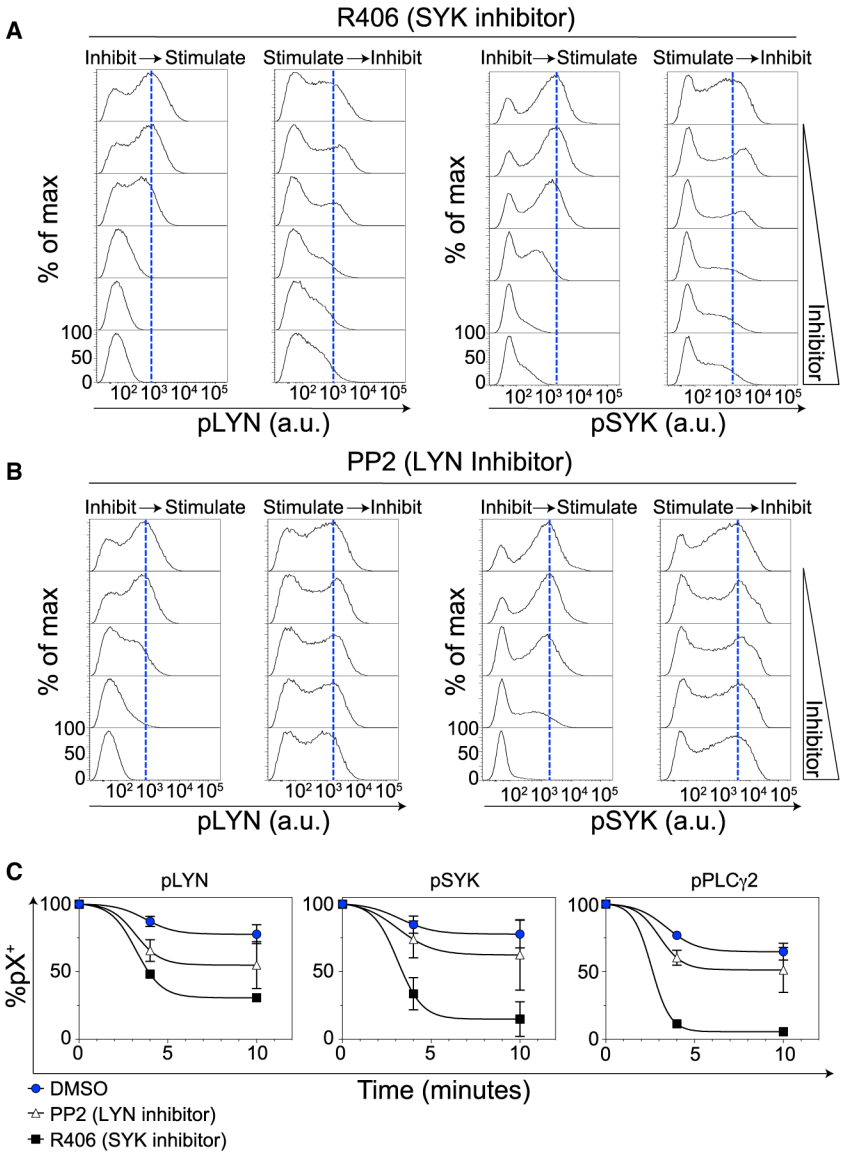

Figure 2. Small-Molecule Inhibitors of SYK and LYN Uncover Positive Feedback in the BCR-Proximal Signaling Pathway

(A and B) Histograms of pLYN (left two columns) and pSYK (right two columns) following H_2O_2 stimulation under increasing doses of the SYK inhibitor R406 (A) and the LYN inhibitor PP2 (B). "Inhibit-Stimulate" columns indicate that cells were pre-treated with inhibitor for 10 min, followed by stimulation with 30 mM H_2O_2 for 4 min. "Stimulate-Inhibit" columns indicate that cells were first stimulated with 30 mM H_2O_2 for 4 min, followed by treatment with inhibitor for 10 min before fixation. Range of R406 concentrations, 10 nM–100 μM; range of PP2 concentrations, 100 nM–100 μM. The data are representative of four experiments. The blue dashed lines indicate the mode of the digitally positive pLYN or pSYK peak within the DMSO-only condition (top plot of each column). a.u., amplitude units.

(C) $\%pLYN^+$, $\%pSYK^+$, and $\%pPLC\gamma2^+$ B cells after H_2O_2 stimulation for 4 min, followed by incubation in stimulation-free media. N = 2 CLL donors. Blue circles, DMSO (vehicle

control). White triangles, PP2 (LYN inhibitor) at 10 μM. Black squares, R406 (SYK inhibitor) at 10 μM.

The data are represented as means ± SEMs. See also Figure S2.

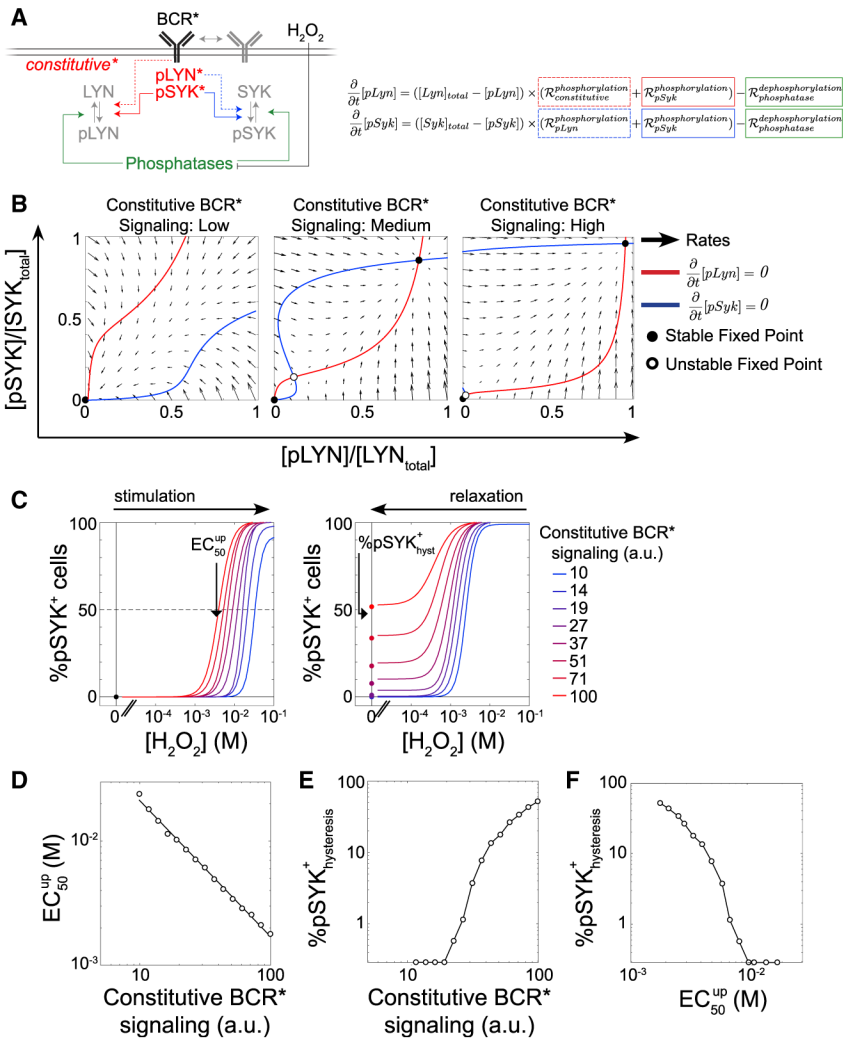

Figure 3. Computational Modeling of B Cell Signaling Uncovers Constitutive BCR Activation as a Dominant Regulator of Hypersensitivity and Hysteresis

(A) Left, schematic of activation of BCR-proximal kinases upon the inhibition of phosphatases by H_2O_2. Right, a set of model equations.

(B) Phase space of LYN and SYK phosphorylation illustrates how bistability (two stable fixed points separated by one unstable fixed point) emerges at intermediate levels of constitutive BCR signaling. The red line represents pLYN nullcline; the blue line represents pSYK nullcline. Filled circles, stable fixed points; open circles, unstable fixed points; arrows, time derivatives for the vector (pLYN, pSYK). Low BCR* signaling, 10 amplitude units (a.u.); medium BCR* signaling, 33 a.u.; high BCR* signaling, 100 a.u. Modeled [H_2O_2] = 10^{-3} M.

(C) Model simulations of experimental data presented in Figure 1C. Left, EC_{50}^{up}; right, steady-state relaxation following stimulation, yielding $\%\ pSYK^{+}_{hysteresis}$. Blue lines, weaker BCR* signaling; red lines, stronger BCR* signaling.

(D and E) Simulated dependency of EC_{50}^{up} (D) and $\%\ pSYK^{+}_{hysteresis}$ (E) for varied levels of constitutive BCR signaling.

(F) Modeled correlation between EC_{50}^{up} and $\%\ pSYK_{hysteresis}^{+}$ over variable BCR signaling.

See also Figure S3 and Table 1.

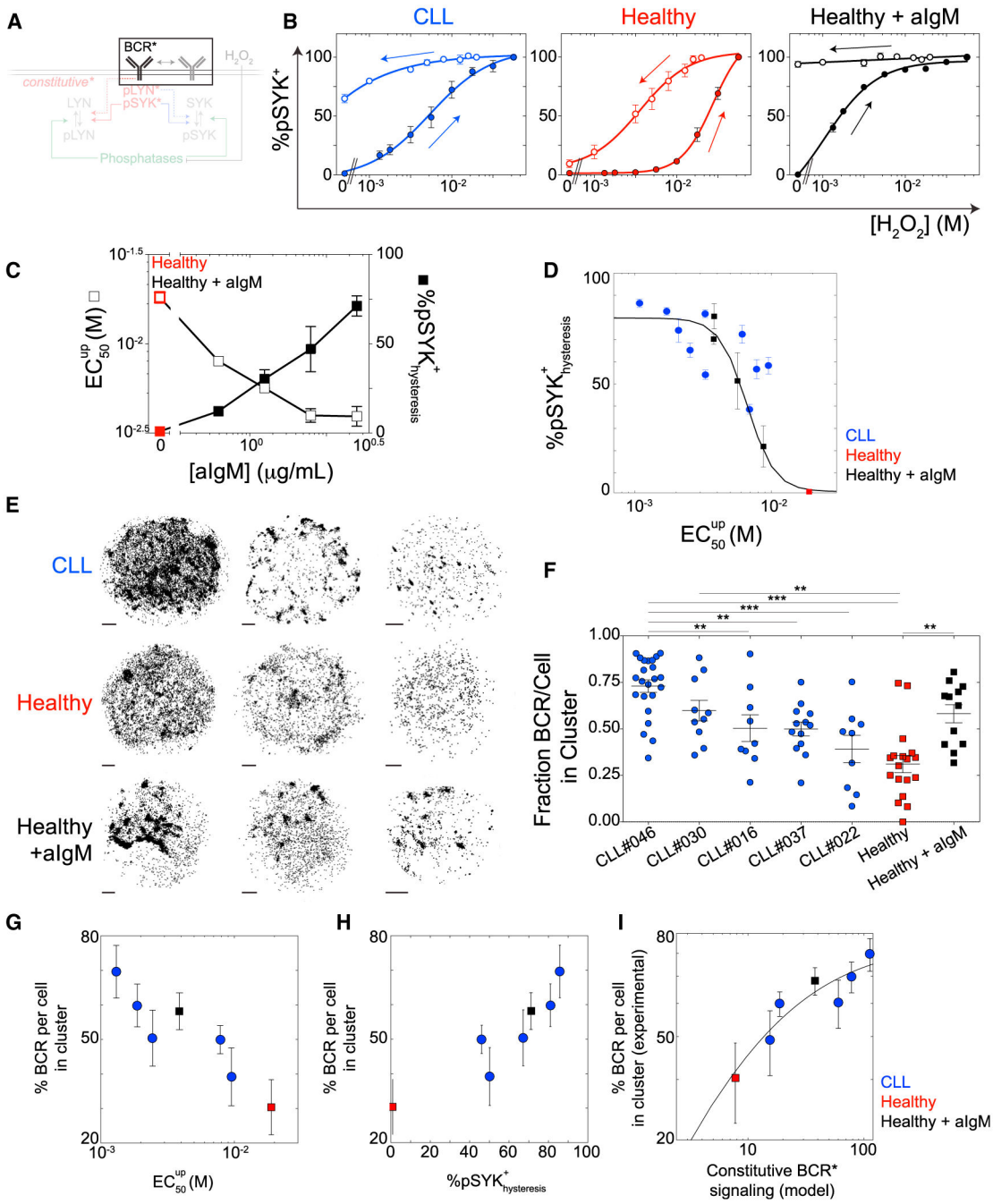

Figure 4. Constitutive BCR Auto-aggregation Explains Altered Signaling in CLL

(A) Schematic of BCR clustering.

(B) %$pSYK^+$ B cells by flow cytometry following H_2O_2 stimulation. Filled circles, stimulation from rest; open circles, relaxation following stimulation. The data represent B cells from n = 3 CLL patients (left, blue), n = 2 healthy donors (center, red), and n = 2 healthy donors concurrently stimulated with 5 μg/mL polyclonal anti-IgM antibody to induce BCR crosslinking (right, black).

(C) EC_{50}^{up} for SYK phosphorylation (left y axis, open squares) and $\%\ pSYK_{hysteresis}^{+}$ following H_2O_2 stimulation and return to stimulation-free media until steady state (30 min, right y axis, filled squares) over a range of anti-IgM (aIgM) doses to induce BCR crosslinking. Red, healthy B cells without aIgM crosslinking; black, healthy B cells exposed to varied doses of aIgM during initial 4-min H_2O_2 stimulation.

(D) Anti-correlation between EC_{50}^{up} and $\%\ pSYK_{hysteresis}^{+}$ within B cells from CLL patients (blue circles), healthy donors (red square), and healthy donor B cells after varied aIgM cross-linking (black squares, range: 0.625–5 μg/mL aIgM). See the model predictions in Figure 3F.

(E) d-STORM for surface IgM demonstrates varied degrees of BCR clustering on B cells from CLL patients (top row), healthy donors (center row), and healthy donors following aIgM-induced crosslinking (bottom row). Three representative cells following preprocessing and point pattern reconstruction in R (see STAR Methods and Figures S4A and S4B). Scale bars: 1 μm.

(F) %BCR per cell in a cluster or complex with another BCR, as imaged by d-STORM. BCR clusters are defined by the presence of at least 1 BCR within a 15-nm radius of a given BCR. The data were collected from 5 CLL donors(blue circles), 2 healthy donors(red squares), and 1 healthy donor pre-treated with 5 μg/mL anti-IgM at 37°C to induce surface clustering (black squares). **$p < 0.01$ and ***$p < 0.001$ by one-way ANOVA and post hoc pairwise comparisons. All of the other pairwise comparisons are non-significant by $p < 0.05$.

(G and H) Correlation between experimentally determined percentage of clustered BCR per cell from d-STORM (y axis) and EC_{50}^{up} (x axis, $p < 0.01$, G) and $\%\ pSYK_{hysteresis}^{+}$ (x axis, $p < 0.01$, H). Blue circles, B cells from CLL donors; red square, healthy donor; black square, healthy donor with BCR clustering induced by 5 μg/mL aIgM at 37°C to induce surface clustering.

(I) Correlation between experimentally determined percentage of clustered BCR and model parameter of constitutive BCR signaling.

The data are represented as means ± SEMs. See also Figure S4.

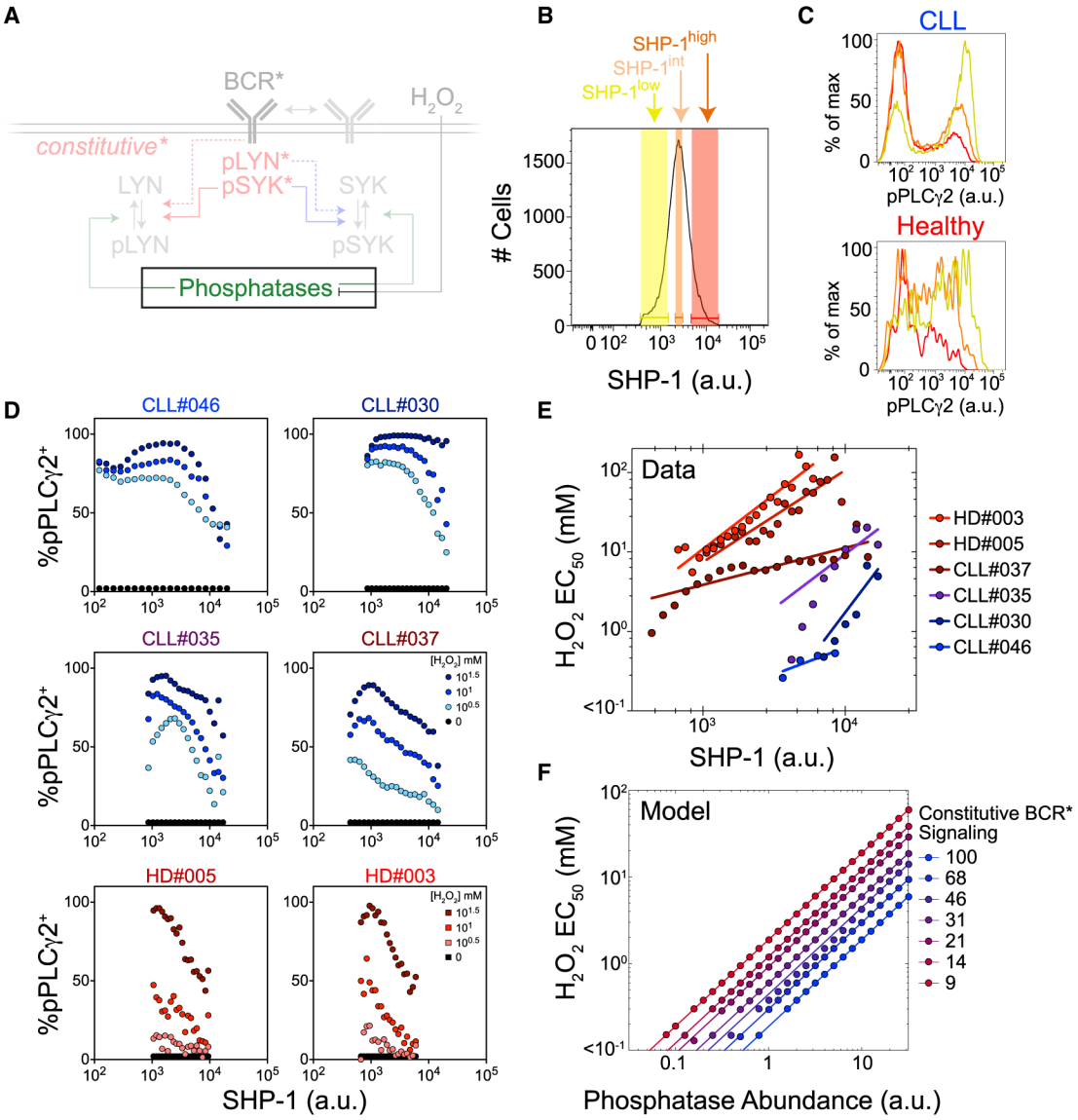

Figure 5. Intra-Donor Variability in B Cell Stimulation Is Explained by Variable SHP-1 Abundances

(A) Schematic for the role of phosphatases in BCR signaling.

(B) Representative histogram of SHP-1 abundance among B cells and definition of three subpopulations based on the differential abundances of SHP-1 protein per cell. SHP-1^{high}, red; SHP-1^{int}, orange; SHP-1^{low}, yellow. a.u., amplitude units.

(C) Representative histograms of pPLCγ2 abundance in B cells from one CLL patient (top) and one healthy donor (bottom) following stimulation with 10 mM H_2O_2. Overlaid traces of red, orange, and yellow histograms reflect subpopulations of B cells gated on SHP-1 abundance (high, intermediate, and low, respectively).

(D) Cell-cell variability analysis by binning on SHP-1 abundance within B cells from four CLL patients and two healthy donors. Cells were exposed for 4 min to a range of H_2O_2 concentrations and analyzed for %pPLCγ2^+ B cells for each dose, binned by SHP-1 abundance (x axis). Darker colors indicate higher concentrations of H_2O_2.

(E) Hill equations were fit for each SHP-1 bin in each donor B cell population. Points represent the fit of EC_{50}^{up} to H_2O_2 stimulation by SHP-1 bin, separated by donor.

(F) Variability in phosphatase abundance (x axis) and BCR signaling (points and lines, blue indicates stronger BCR clustering, red indicates weaker BCR clustering) affect BCR-proximal signaling dynamics, simulated as EC_{50}^{up} to H_2O_2 stimulation (y axis).

See also Figure S5.

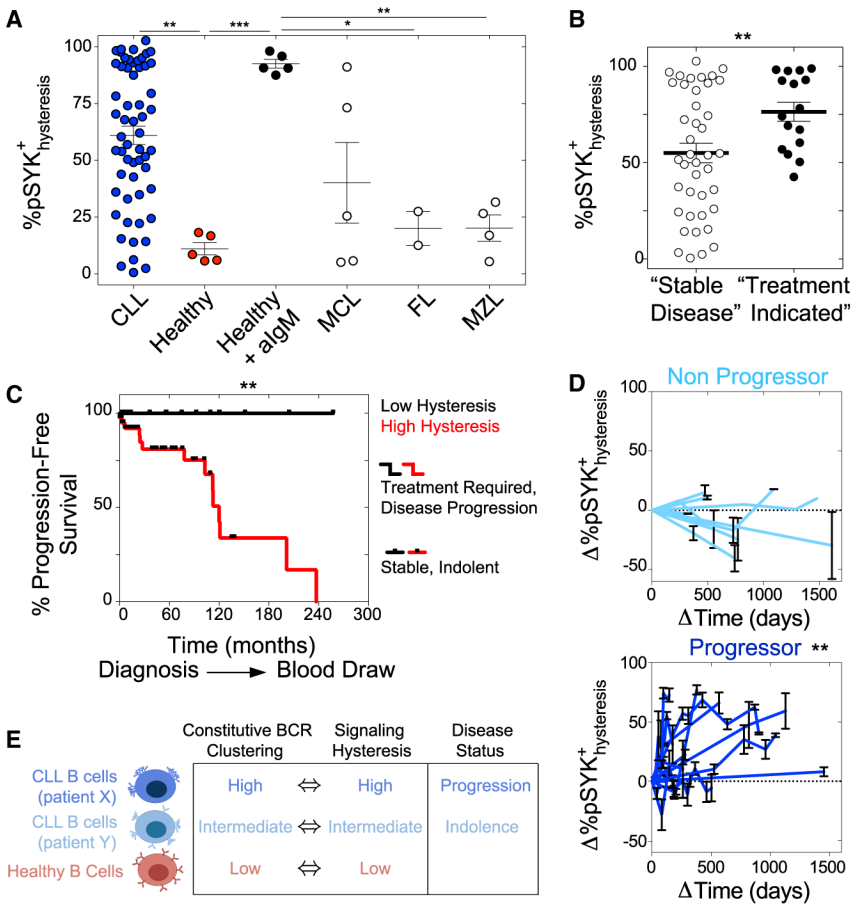

Figure 6. pSYK Hysteresis Correlates with CLL Clinical Status

(A) $\%\ pSYK^{+}_{hysteresis}$ within B cells from healthy donors (red, n = 5), from healthy donor B cells treated with aIgM to induce BCR clustering (black filled, n = 5), B cells from patients with CLL (blue, n = 57), mantle cell lymphoma (MCL, n = 5), follicular lymphoma (FL, n = 2), and marginal zone lymphoma (MZL, n = 4). *p < 0.05, **p < 0.01, and ***p < 0.001 by one-way ANOVA and post hoc pairwise comparisons.

(B) $\%\ pSYK^{+}_{hysteresis}$ within B cells from CLL patients with stable disease (open circles) and patients requiring immediate treatment (black circles), as indicated in the records of patient encounters on the day of the blood draw. **p < 0.01 by Student's t test.

(C) Kaplan-Meier survival curve of progression-free survival among CLL patients from diagnosis to status at blood draw, partitioned by $\%\ pSYK^{+}_{hysteresis}$. "Low Hysteresis": $\%\ pSYK^{+}_{hysteresis}$ < 40%, "High Hysteresis" > 40%. **p < 0.01 by Mantel-Cox test.

(D) Longitudinal analysis of $\%\ pSYK^{+}_{hysteresis}$, assessed at multiple donation time points. Top, untreated CLL patients exhibiting progression-free disease ("Non Progressor"). Bottom, actively treated CLL patients exhibiting progressive disease ("Progressor"). **p < 0.01 by Student's t test.

(E) Model schematic for the variability of constitutive BCR signaling and the pathophysiology of CLL B cells.

See also Figure S6 and Table S1.

Cell Rep. Author manuscript; available in PMC 2021 April 02.

Table 1.

Computational Model Parameters

Parameter	Term	Value	Units	Source/Notes
pSYK phosphorylation rate	k_{cat}^{pSyk}	1.2	s^{-1}	measured (Mukherjee et al., 2013)
pLYN phosphorylation rate	k_{cat}^{pLyn}	3.5	s^{-1}	measured (Mukherjee et al., 2013)
uLYN phosphorylation rate		10^{-7}	s^{-1}	measured (Barua et al., 2012)
PTPx dephosphorylation rate	k_{cat}^{P}	0.12	s^{-1}	measured (Zhang et al., 2003)
uSYK BCR binding k_{on}		9.3×10^{-5}	$s^{-1}molecules^{-1}$	measured (Tsang et al., 2008)
uSYK BCR binding k_{off}		10	s^{-1}	measured (Tsang et al., 2008)
K_m uSYK BCR-pSYK	$K_m^{pSyk-Syk}$	1.2×10^5	molecules	
K_m uSYK BCR-pLYN	$K_m^{pLyn-Syk}$	1.4×10^5	molecules	
pSYK BCR binding k_{on}	$k_{on}^{pSyk-BCR}$	4.6×10^{-5}	s^{-1} $molecules^{-1}$	measured (Tsang et al., 2008)
pSYK BCR binding k_{off}	$k_{off}^{pSyk-BCR}$	0.1	s^{-1}	measured (Tsang et al., 2008)
uLYN BCR binding k_{on}		8.8×10^{-5}	s^{-1} $molecules^{-1}$	measured (Mukherjee et al., 2013; Altan-Bonnet and Germain, 2005)
uLYN BCR binding k_{off}		5.9	s^{-1}	measured (Mukherjee et al., 2013; Altan-Bonnet and Germain, 2005)
K_m uLYN BCR-pSYK	$K_m^{pSyk-Lyn}$	8.1×10^4	molecules	
K_m LYN BCR	$K_m^{BCR-Lyn}$	6.8×10^4	molecules	
pLYN BCR binding k_{on}	$k_{on}^{pLyn-BCR}$	8.8×10^{-5}	s^{-1} $molecules^{-1}$	measured (Mukherjee et al., 2013; Altan-Bonnet and Germain, 2005)
pLYN BCR binding k_{off}	$k_{off}^{pLyn-BCR}$	0.59	s^{-1}	Measured (Mukherjee et al., 2013; Altan-Bonnet and Germain, 2005)
Phosphatase oxidation rate	$k_{oxidize}$	150	s^{-1}	measured (Figure S1)
Phosphatase reduction rate	k_{reduce}	0.002	s^{-1}	measured (Figure S1)
Phosphatase K_m	K_m^p	54	molecules	measured, assume BCR-SHP1 K_m is representative (Mukherjee et al., 2013)
H_2O_2	$[H_2O_2]$	[0, 1]	dimensionless	fit (Figure S1)
Total SYK	$[Syk]_{total}$	2,390	molecules	measured and calculated for membrane-proximal reaction space of 5.6 μm^3, 427 molecules/μm^2 (Mukherjee et al., 2013)

Parameter	Term	Value	Units	Source/Notes
C.V. SYK		0.59	dimensionless	measured (Figure S3)
Total LYN	$[Lyn]_{total}$	3,120	molecules	measured and calculated for membrane-proximal reaction space of 5.6 μm^3, 427 molecules/μm^2 (Mukherjee et al., 2013)
C.V. LYN		0.64	dimensionless	measured (Figure S3)
Total PTPx	$[PTPx]_{total}$	2,180	molecules	measured and calculated for membrane-proximal reaction space of 5.6 μm^3, 427 molecules/μm^2 (Mukherjee et al., 2013)
C.V. SHP1		0.55	dimensionless	measured (Figure S3)
Total BCR		31,750	molecules	measured (Mukherjee et al., 2013; Tsourkas et al., 2007)
Spearman's ρ (pSYK, pLYN)		0.96	dimensionless	measured (Figure S3)

KEY RESOURCES TABLE

REAGENT or RESOURCE	SOURCE	IDENTIFIER
Antibodies		
polyclonal Goat anti-Human anti-IgM F(ab')2	Invitrogen	16-5099-85; RRID:AB_2573090
pLck/Lyn (Alexa Fluor 647, pY505) [Clone 4/LCK-Y505]	BD Biosciences	558577; RRID:AB_647134
pSyk (PE, pY348) [Clone I120-722]	BD Biosciences	558529; RRID:AB_647247
pPlcγ2 (Alexa Fluor 488, pY759)[Clone K86-689.37]	BD Biosciences	558507; RRID:AB_647094
Pacific Blue-conjugated anti-CD3 (clone UCHT1)	BD Biosciences	558117; RRID:AB_397038
PerCPCy5.5 conjugated anti-CD20 (clone H1)	BD Biosciences	558021; RRID:AB_396990
PE-Cy7-conjugated anti-CD5 (clone L17F12)	BD Biosciences	348790; RRID:AB_400380
Donkey anti-Goat IgG A647	Jackson Immunochemicals	705-605-147; RRID:AB_2340437
SH-PTP1 Antibody (clone C-19)	Santa Cruz Biotechnology	sc-287; RRID:AB_2173829
Mouse anti-Human HLA-DP (Clone WR18)	Abd Serotec	MCA477; RRID:AB_322101
Biological Samples		
Peripheral Blood Mononuclear Cells (PBMC) from Blood biopsies of: 57 CLL patients, 14 healthy donors, 28 Mantle Cell Lymphoma (MCL) patients, 2 Follicular Lymphoma (FL) patients, and 4 Marginal Zone Lymphoma (MZL) patients.	Memorial Sloan Kettering Lymphoma Service	N/A
Chemicals, Peptides, and Recombinant Proteins		
Ficoll-Paque Plus	GE Healthcare	17-1440-02
Sodium Orthovanadate	Sigma	S6508
Hydrogen Peroxide (H_2O_2)	Sigma	H1009
Paraformaldehyde	BD Biosciences	554655
PP2 Src Inhibitor	Sigma	CAS 172889-27-9 I 529573
R406 Syk inhibitor	Sigma	CAS 841290-80-0 I 5058190001
Mouse gamma globulin	Jackson Immunochemicals	015000002
Recombinant human IgM	Sigma	I8260
Fetal Bovine Serum	Thermo Fisher Scientific	26140087
RPMI 1640	Thermo Fisher Scientific	11875093
NaCl	Sigma	S3014
Glucose oxidase	Sigma	G7141
Catalase	Sigma	C40
Glucose	Sigma	G8270
MEA (β-mercaptoethylamine)	Sigma	30070
Critical Commercial Assays		
2′,7'-dichlorofluorescin diacetate (DCFDA)	Abcam	ab113851
Magnetic Protein A coated beads (Dynabeads)	Life Technologies	10001D
Software and Algorithms		
ZEN (black edition + PALM module) for ELYRA PS.1 system	Carl Zeiss GmBH	https://www.zeiss.com/microscopy/us/products/microscope-software/zen.html
R Project for Statistical Computing	The R Project	https://www.r-project.org/
MATLAB	MathWorks	https://www.mathworks.com/

REAGENT or RESOURCE	SOURCE	IDENTIFIER
FlowJo	TreeStar	https://www.flowjo.com/
Prism	GraphPad	https://www.graphpad.com/scientific-software/prism/